

Coherent control calculations for helium atom in short and intensive XUV laser pulses

I.F. Barna^a

Institute for Theoretical Physics, Vienna University of Technology, Wiedner Hauptstr. 8-10, 1040 Vienna, Austria

Received 24 September 2004 / Received in final form 17 March 2005

Published online 26 April 2005 – © EDP Sciences, Società Italiana di Fisica, Springer-Verlag 2005

Abstract. Coherent control calculations are presented for helium. With the help of a genetic algorithm (GA) phase-modulated extreme ultra violet (XUV) laser pulses were controlled to maximize or minimize the non-resonant two-photon $1s1s \rightarrow 1s3s$ excitation. Linearly polarized laser pulses were chosen at the frequency of 0.4 a.u. with a duration of about 15 fs and 10^{14} Wcm⁻² peak intensity. We verified the theory that an antisymmetric spectral phase around the two-photon resonance frequency maximizes the transition probability. Dark pulses which do not excite the system at all have however symmetric spectral phases around the two-photon resonance frequency.

PACS. 32.80.Wr Other multiphoton processes – 32.80.Qk Coherent control of atomic interactions with photons – 31.15.Ar Ab initio calculations

1 Introduction

It is experimentally possible with tailored femtosecond laser pulses from a computer-controlled pulse shaper [1] to optimise the branching ratios of different chemical reactions [2]. These experiments are based on the original ideas of optimal control theory [3–5] later expanded by [8] into a hypothetical experimental setup making it possible to solve and control the Schrödinger equation in real time. There are basically two different controlling schemes exist. The ‘pump-dump control’ developed by Tannor and Rice [6], which relies on the timing between two laser pulses to manipulate the quantum dynamics such as the fracturing of specific bonds in the given molecule. The second control mechanism was introduced by Shapiro and Brumer [7] and is based on quantum interference of different light-induced reaction paths. Further details including references about pulse-shaping and coherent control mechanisms are given in the review by [9].

Here we report on quantum interference coherent control calculations with short and intensive XUV pulses which may attract interest in future Free-Electron-Laser (FEL) experiments. We implement our coupled-channel method for controlling laser driven helium atoms. So far, the method has been successfully applied to ionization of helium in heavy ion collisions [10] and photoionization of helium [11] in the 0.2–1.2 a.u. photon energy regime. In our method we can approximate the discrete and continuum parts of the spectrum of helium with sufficient accuracy. We investigate non-resonant two-photon $1s1s \rightarrow 1s3s$ excitation in helium. Resonant two-photon

excitation processes in atoms have been extensively studied, both experimentally [13] and theoretically [14–16].

In this study we generalise the theory of [15,16] maximizing and minimizing non-resonant two-photon transition probabilities. Following the experimental set-ups available today, we apply phase modulation with the genetic algorithm (GA) [17] as an optimisation procedure to create the best interacting and most ineffective pulses (dark pulses) for the $1s1s \rightarrow 1s3s$ excitation. A detailed analysis about the evolutionary algorithms in optimal control studies was presented in [18]. Further details about different learning algorithms can be found in reference [19].

Atomic units are used throughout the paper unless otherwise indicated.

2 Theory

To describe controlled laser-driven atomic processes in helium we solve the coupled-channel differential equation system for the time-dependent wavefunction expansion coefficients

$$\frac{da_k(t)}{dt} = -i \sum_{j=1}^N V_{kj}(t) e^{i(E_k - E_j)t} a_j(t) \quad (k = 1, \dots, N), \quad (1)$$

where E_k and E_i are the channel eigenvalues of the unperturbed spin-independent helium Hamiltonian and $V_{kj}(t)$ is the coupling matrix element

$$V_{kj}(t) = \langle \Phi_k | \hat{V}(t) | \Phi_j \rangle. \quad (2)$$

^a e-mail: barna@concord.itp.tuwien.ac.at

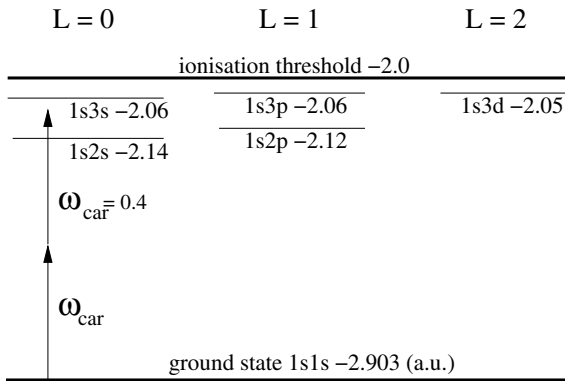


Fig. 1. The low-lying excited states of the helium atom with the non-resonant frequency of the laser pulse.

The eigenfunctions $\{\Phi_j\}$ are obtained by diagonalising the helium Hamiltonian in a configuration interaction basis of orthogonal symmetrized two-particle wavefunctions. $V(t)$ is the dipole interaction operator between the laser pulse and the atomic electrons, and will be specified later on. For the single-particle wavefunctions we use an angular representation with spherical harmonics Y_{lm} with hydrogen-like radial Slater functions and regular Coulomb wave packets. Further technical details can be found in [11] or [12].

In our basis 40 channels were used with angular momenta $L = 0, 1, 2$ up to the second ionization threshold of helium. According to test calculations if the density of states reached the required level (for $\omega_{car} = 0.4$ a.u. in energy range $\approx [-3 : 0]$ means at least 8 states per angular momenta), the optimisation process becomes stable. Beyond the $1s1s$ and $1s3s$ states different bound states were included such as $1s2s$, $1s4s$, $1s2p$ or $2s2s$. The list of the bound states can be found in reference [11]. Figure 1 shows some low-lying excited states in the helium atom, together with the applied non-resonant laser pulse frequency.

The probabilities for the transitions into final helium states j after the pulse are simply given by

$$P_j = |a_j(t \rightarrow +\infty)|^2. \quad (3)$$

When a state-selective excitation probability is controlled then the corresponding channel is considered.

To describe the external field we restrict ourselves to linearly polarized laser pulses parallel to the z -axis. The length gauge with the dipole approximation is applied as

$$V(t) = \sum_{i=1,2} \mathbf{E}(t) \cdot \mathbf{r}_i \quad (4)$$

where $\mathbf{E}(t)$ is the electric field strength of the laser and \mathbf{r}_i is the coordinate of the electrons. To start phase modulation a transform-limited pulse spectrum is needed. We calculate the Fast-Fourier Transformation (FFT) of a narrow Gaussian pulse

$$\mathbf{E}(t) = E_0 \exp \left[-a(T/2 - t)^2 \right] \sin(\omega t) \mathbf{e}_z \quad (5)$$

where ω is the carrier frequency. The parameters a help us to fix the width of the pulse and T shifts it into the middle

of the required time window. For $\omega = 0.4$ carrier frequency we used the following parameters: $T = 188$ a.u. (4.5 fs) $E_0 = 0.091$ a.u. ($I = 2.92 \times 10^{14}$ W/cm²) and $a = 0.02$ with 512 different time points. To have stable numerics we embedded this short pulse between two $15T$ long zero padded intervals using 15872 time points. From this large number of Fourier frequencies 128–130 relevant frequencies emerged following the experimental setup of [2]. Phase modulation can be defined as:

$$\tilde{E}(\omega) = E(\omega)e^{if(\omega)} \quad (6)$$

where $E(\omega)$ is the spectrum of the initial pulse and $f(\omega)$ is the phase function. In our case $f(\omega)$ must be a continuous function without any sharp peaks or singularities. To avoid numerical difficulties, only eleven Fourier coefficients are modulated where the phase function is a randomly given real number in the $[-\pi : \pi]$ interval. These eleven points were equidistantly distributed. To get the phase function between these given points, a spline interpolation is applied. This procedure reduces the number of free parameters, accelerating the optimisation algorithm and giving a quite general and flat phase function which is comparable to the experimental results of [20]. Our investigation shows that this realization of phase modulation with a FFT algorithm is robust and reliable for control calculations which is in agreement with [18].

Phase modulation preserves pulse energy conservation and needs no renormalization. Pulses with modulation have a longer duration and lower peak intensity than the initial narrow Gaussian pulse. Our phase modulation algorithm may give pulses with different length up to $15T$ (67.5 fs). The length of these pulses are defined through 99.9 percent energy conservation, integrating the intensity and comparing to the initial Gaussian pulse. To accelerate the time propagation of the coupled-channels equations we cut and integrate the relevant time window only (see Fig. 3). For time propagation we use a Runge-Kutta-Fehlberg method of fifth-order embedding an automatic time-step regulation [12].

To optimise the free phases we apply the genetic algorithm. The GA represents each possible solution, or individual, with a string of bits, termed a chromosome. For example, a possible phase is represented as [01101111]. (For the sake of clarity, we assume that each parameter can only take 2^8 values in this example.) The first generation of individuals is selected randomly. Typically, we use a population with 20 individuals which is about a factor two larger than the number of the optimisable variables. For each generation, the following steps are carried out: (i) all the individuals are evaluated and assigned a fitness value. In our case, we calculate the ionization or state selective excitation probability resulting from each parameter configuration, calling it a fitness value. The next generation of individuals is chosen by applying the three GA operators: selection, mutation and crossover. (ii) The selection operator chooses which of the individuals from the present generation will be transferred to the next generation. The individuals are ranked according to their fitness, and then selected randomly with a certain probability based on

the fitness. A fit individual thus receives a high probability and can be selected many times, while a low-fitness individuals may not be selected at all. (iii) The mutation operator, which is very seldom used, selects a few individuals and replaces one (randomly selected) bit in chromosome by randomly 0 or 1 (i.e. creating the chromosomes [11010111] from [11000011].) (iv) The crossover operator takes two individuals at a time and exchanges part of their chromosomes. For example, the two chromosomes [00110100] and [11100111] can create the chromosomes [00110111] and [11100100]. The use of the mutation and crossover operators ensures that the GA does not get trapped in a local minimum or maximum. The fittest individuals, however, always survive to the next generation which is called elitism. The steps (i–iv) are then repeated until convergence is achieved.

3 Results

Our coupled-channel method was tested and verified for photon energies between 0.2 and 1.2 a.u. The applied pulse duration was 3.8 fs. Above this energy range, we enter the working range of the planned Free Electron Laser (FEL) where only single photon processes come into play, leaving no room for control. On the other hand, with photon energies below 0.2 a.u. we enter into a range where our method becomes inaccurate due to the large number of absorbed photons. The carrier frequency of our pulse is now $\omega_{car} = 0.4$ a.u., which is slightly smaller than the resonant two-photon $1s1s \rightarrow 1s3s$ photon energy, which is 0.42 a.u. ($E_{1s1s} = -2.903$ a.u. and $E_{1s3s} = -2.06$ a.u.) The carrier is now non-resonant for the $1s1s \rightarrow 1s3s$ two-photon excitation process.

We chose eleven free phases covering the spectrum of the pulse to optimise. If we slightly enhanced the number of the free parameters, (free phases e.g. from 11 to 22) then the shape of the pulses may differ, but the properties of the wave packet remains the same. If we drastically enhanced the number of the free phases (e.g. from 22 up to 64), then the phase function became oscillating, the duration of the pulse became very long and the time propagation took much more time. Due to the energy conservation, long pulses have low peak intensities which bring down the transition probabilities. And at last, the optimisation problem with a large number of parameters once again requires much time. These experiences confirm the statements of [18].

We used 20 different pulses in our calculations per generation (population size), and let the process run through 40 generations to achieve convergence. This means that 800 different pulses were checked to find the most favorable ones. The value used for the permutation probability was ($\approx 1/\text{population size}$) 0.05, for the crossover probability was 0.4, and for creeping probability was 0.06, matching the recommendation of the routine [17].

Figure 2 shows the convergence properties of our calculations. The filled circles present the convergence of the best pulse, and the hollow triangles show convergence of the dark pulse, respectively. We found that optimisation

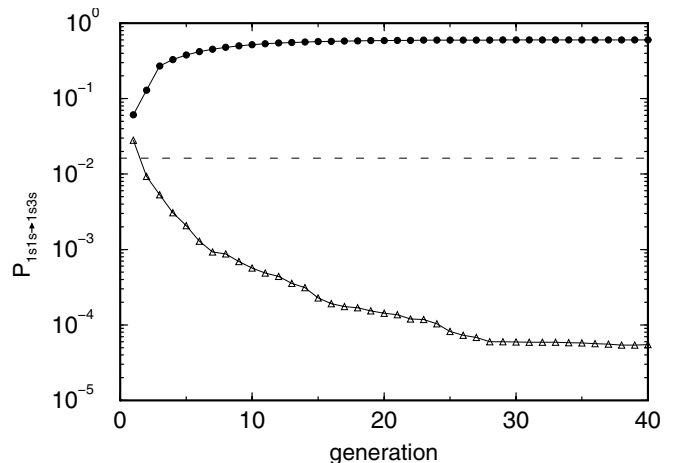


Fig. 2. The convergence of the genetic algorithm for the $1s1s \rightarrow 1s3s$ transition. The full circles show the excitation probabilities of the best pulse, and the hollow triangles the dark pulse. The solid lines are for guiding the eyes. The dashed line shows the result of the Gaussian pulse.

for the best pulse converges much faster and results in smaller gain than optimisation for dark pulses for loss. The Gaussian pulse equation (5) gives an excitation probability of about 0.02. The maximized excitation probability is 0.6 which means a factor of 30 in gain. The darkest pulse causes excitation with a probability of $P = 5.37 \times 10^{-5}$, which is a factor of 372 in loss. Theoretically, dark pulses may exist with zero two-photon excitation probability. We could not find such pulses during our investigation.

We started two optimisation procedure, one for the best and one for the worst pulse with different random pulses which is why the first generations have different results.

Figure 3a shows the electric field strength of the transform limited Gaussian pulse equation (5). Figures 3b and 3c present the electric field of the optimised best and dark pulses, respectively. The best pulse has a length of about 625 a.u. (15 fs) and the worst pulse is about a factor of two longer. Note that these pulses are not the absolute best or darkest pulses which exist, but optimised enough, to show the feature of the non-resonant two-photon coherent control mechanism. These two pulses are the most extreme individuals from the last generations. We analyzed our results with the help of the second-order time-dependent perturbation theory formula of [15]. If the two-photon process is non-resonant, then the probability of inducing a transition to the excited state by the laser pulse is proportional to:

$$S_2 = \left| \int_{-\infty}^{+\infty} \tilde{E}(\omega_0 + \Omega) \tilde{E}(\omega_0 - \Omega) d\Omega \right|^2 = \left| \int_{-\infty}^{+\infty} E(\omega_0 + \Omega) E(\omega_0 - \Omega) e^{i\{f(\omega_0 + \Omega) + f(\omega_0 - \Omega)\}} d\Omega \right|^2, \quad (7)$$

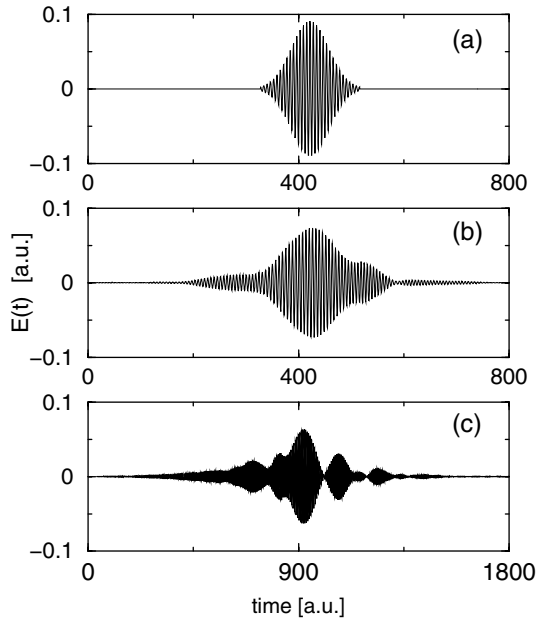


Fig. 3. Electric field strength of the applied pulses. (a) The transform-limited initial pulse, (b) optimised best pulse and (c) the optimised dark pulse.

where $\tilde{E}(\omega) = E(\omega)e^{if(\omega)}$ is the Fourier transform of the electric field of the excitation pulse $E(t)$, and $E(\omega)$ and $f(\omega)$ are the spectral amplitude and the spectral phase, respectively. Ω is an arbitrary frequency close to the resonant frequency inside the spectrum of the pulse. Equation (7) clearly reflects the fact that two-photon transitions occur for all pairs the frequency when $\omega_1 + \omega_2 = 2\omega_0$, and ω_1, ω_2 lie within the spectrum of the exciting pulse. For a given pulse spectrum it is obvious that S_2 is maximized by the transform limited pulse with minimal time duration with $f(\omega) = 0$. Consider a pulse with the same energy and power spectrum, but having any antisymmetric spectral phase distribution around the resonant two-photon frequency ω_0 , $f(\omega_0 + \Omega) = -f(\omega_0 - \Omega)$. The phase terms cancel each other, and the two-photon transition probability is independent of the spectral phase. It is clear that an infinite number of antisymmetric phase functions exist which unambiguously determine the pulse shape. Figure 4a presents the phase function of the optimised best pulse, and Figure 4b the worst pulse respectively. The two arrows mark the carrier ω_{car} and the resonance ω_0 frequencies. Note that the phase function of the best pulse has clean antisymmetry around the two-photon resonance frequency $\omega_0 = 0.42$. Contrary to this, the dark pulse has a clean symmetry around ω_0 . If we tune or detune the ω_{car} carrier frequency relative to the resonance frequency ω_0 , then the symmetry properties of the best and worst (dark) pulses remain the same. Of course, the gain or loss through optimisation will be changed. If the carrier frequency of the pulse is equal to the two-photon resonant frequency $\omega_{car} = \omega_0$ then the transform limited Gaussian pulse is one of the best pulse. However, pulses with symmetric phase functions are com-

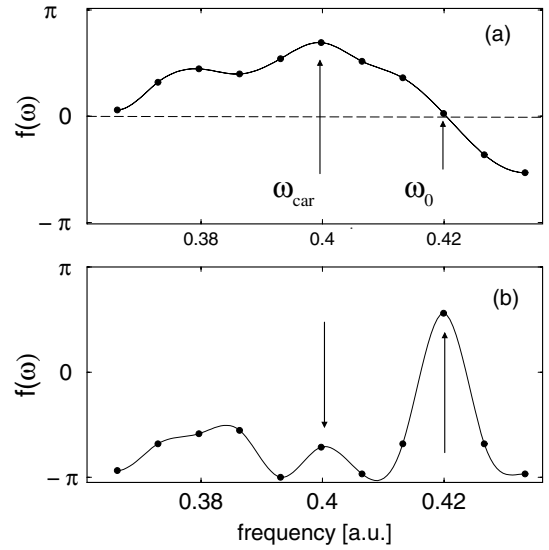


Fig. 4. Two phase functions $f(\omega)$, (a) of the optimised best and, (b) the optimised dark pulse.

pletely ‘dark’ producing no $1s3s$ excitation at all. We did calculations for the $1s1s \rightarrow 1s3d$ non-resonant two-photon transitions as well. The energy difference between the $1s3s$ and $1s3d$ energy levels is minimal, ($E_{1s3s} = -2.06$ a.u. and $E_{1s3d} = -2.05$ a.u.), which is why the same pulses were taken. The results did not show significant deviation from the results analyzed above.

4 Summary and outlook

We have presented coherent control calculations for the helium atom in short and intensive XUV laser pulses. The optimised pulses have a peak intensity of about 10^{14} Wcm $^{-2}$, duration of a 15–30 fs and carrier frequency of 0.4 a.u.

With the help of the genetic algorithm, the spectral phases of the pulses were controlled for the non-resonant two-photon $1s1s \rightarrow 1s3s$ excitation. The second-order perturbation theory for two-photon excitation processes helped us to understand and explain the gain and loss of the optimisation.

Coherent control experiments work in the visible or infrared frequency range nowadays. Our calculations were done in the XUV energy regime with the hope that the rapid development of femtosecond laser technology will make this pulses realizable in the near future.

We thank Dr. A. Becker and Professor J.M. Rost for fruitful discussions and constructive ideas and Prof. J. Burgdörfer who helped us to improve the manuscript. This work was supported by SFB 016-FWF and EU-HITRAP Project Number HPRI-CT-2001-50067.

References

1. A.M. Weiner, *Prog. Quant. Electr.* **19**, 161 (1995)
2. T. Brixner, N.H. Darmrauer, G. Gerber, *Adv. At. Mol. Opt. Phys.* **46**, 1 (2001)
3. S. Shi, A. Woody, H. Rabitz, *J. Chem. Phys.* **88**, 6870 (1988)
4. A. Pierce, M. Dahleh, H. Rabitz, *Phys. Rev. A* **37**, 4950 (1988)
5. R. Kosloff, S. Rice, P. Gaspard, S. Tersigi, D.J. Tannor, *Chem. Phys.* **139**, 201 (1989)
6. D.J. Tannor, S.A. Rice, *J. Chem. Phys.* **85**, 5805 (1986)
7. M. Shapiro, P. Brumer, *J. Chem. Phys.* **84**, 4103 (1986)
8. R.S. Judson, H. Rabitz, *Phys. Rev. Lett.* **68**, 1500 (1992)
9. D. Goswami, *Phys. Rep.* **374**, 385 (2002)
10. I.F. Barna, N. Grün, W. Scheid, *Eur. Phys. J. D* **25**, 239 (2003)
11. I.F. Barna, J.M. Rost, *Eur. Phys. J. D* **27**, 287 (2003)
12. I.F. Barna, *Ionization of helium in relativistic heavy-ion collisions*, Doctoral thesis, University Giessen (2002) "Giessener Elektronische Bibliothek"
<http://geb.uni-giessen.de/geb/volltexte/2003/1036>
13. R. Teets, J. Eckstein, T.W. Hänsch, *Phys. Rev. Lett.* **38**, 760 (1977)
14. V. Blanchet, C. Nicole, M.-A. Bouchene, B. Girard, *Phys. Rev. Lett.* **78**, 2716 (1997)
15. D. Meshulach, Y. Silberberg, *Nature* **396**, 239 (1998)
16. D. Meshulach, Y. Silberberg, *Phys. Rev. A* **60**, 1287 (1999)
17. D.L. Carroll, *Free Genetic Algorithm Driver*
<http://cuaerospace.com/carroll/ga.html>
18. D. Zeidler, S. Frey, K.-L. Kompa, M. Motzkus, *Phys. Rev. A* **64**, 023420-1 (2001)
19. P. Mars, J.R. Chen, R. Nambiar, *Learning Algorithms* (CRS Press Inc., 1996)
20. T. Brixner, M. Strehle, G. Gerber, *Appl. Phys. B* **68**, 281 (1999)